

A phase field model with arbitrary misorientation dependence of grain boundary energy

Philip Staublin^{a,*}, Yuri Mishin^b, and Peter W. Voorhees^{c,d,e}

March 17, 2026

^aDepartment of Materials Science and Engineering
University of Michigan
2300 Hayward Street
Ann Arbor, MI 48109

^bDepartment of Physics and Astronomy
George Mason University
4400 University Drive, MSN 3F3
Fairfax, VA 22030-4444

^cDepartment of Applied Physics and Materials Science
California Institute of Technology
1200 East California Boulevard
Pasadena, CA 91125

^dDepartment of Materials Science and Engineering
Northwestern University
2220 Campus Drive
Evanston, IL 60202

^eDepartment of Engineering Sciences and Applied Mathematics
Northwestern University
2220 Campus Drive
Evanston, IL 60202

*Corresponding author; pstaublin@u.northwestern.edu

1 **Abstract**

2 Grain growth in polycrystals is often simulated using orientation-field models, which employ
3 a field to represent the local orientation of the crystal lattice. These models can be chal-
4 lenging to represent a realistic misorientation dependence of grain boundary free energy. We
5 prove that existing orientation-field models, in general, cannot reproduce a decrease in the
6 grain boundary free energy with a increasing misorientation angle, demonstrating a signifi-
7 cant limitation of previous models in applications to polycrystalline materials. To overcome
8 this limitation, we propose a modification to the Kobayashi-Warren-Carter model for grain
9 growth wherein the coefficients of the free-energy functional become functions of the mis-
10 orientation between the grains, which is a non-local quantity. Due to this modification, an
11 arbitrary dependence of the grain boundary free energy on the misorientation can be embed-
12 ded in the model. We propose calculating the non-local misorientation by interpolating the
13 orientation field at a fixed distance in both directions along the local grain boundary normal
14 vector. The capabilities of the model are demonstrated by introduction of a sharp cusp to
15 the misorientation dependent grain boundary free energy. Finally, we propose an extension
16 of the model to three dimensions.

17 *Keywords.* Grain boundary, Grain growth, Phase field model, Orientation-field model

1 Introduction

Orientation-field models are a class of phase-field models that simulate polycrystalline systems by treating the local crystal orientation as a field variable [1–8]. In contrast to the multi-order-parameter [9–11] and multi-phase-field models [12–20], which assign a distinct field variable to each crystal orientation, the orientation-field models have only a single order parameter coupled to a continuous orientation field. Orientation-field models have the computational advantage of simulating any number of grains without scaling the number of required order parameters; in addition, the triple junction dynamics reproduces the results of classical theory [7]. In order to leverage the advantages of the orientation-field models for practical problems, such as the extraction of information from experimental tomographic measurements of grain growth [21], the relationship between model parameters and the properties of grain boundaries in the model must be clearly defined.

There are two families of orientation-field models, differing by the manner in which they ensure localized grain boundaries. The Kobayashi-Warren-Carter model includes two terms dependent on the orientation field θ in the free energy density: one depends on $|\nabla\theta|$ while the second depends on $|\nabla\theta|^2$. At constant temperature, and without an inclination dependence of the grain boundary (GB) energy, the free energy of the model in a domain Ω is [3]

$$F[\phi, \theta] = \int_{\Omega} \left[V(\phi) + \frac{\alpha^2}{2} |\nabla\phi|^2 + sg(\phi)|\nabla\theta| + \frac{\epsilon^2}{2} h(\phi)|\nabla\theta|^2 \right] dV. \quad (1)$$

The coupling functions $g(\phi)$ and $h(\phi)$ increase monotonically, with the influence of orienta-

tion vanishing in the liquid phase ($\phi = 0$). The model parameters α , s , and ϵ determine the GB energy¹ by adjusting the strength of the coupling between ϕ and θ . The choice of model parameters affects a critical misorientation at which the GB width diverges, effectively resulting in melting of the boundary. The presence of the first order term results in stationary
40 solutions for the GB profile.

The second family of models, the HMP model after Henry, Mellenthin, and Plapp [4], omits the first-order gradient term in θ , favoring a singular coupling function on the $|\nabla\theta|^2$ term to localize the boundaries. The free energy in the HMP model is defined by

$$F[\phi, \theta] = \int_{\Omega} \left[\frac{W_{\phi}^2}{2} |\nabla\phi|^2 + HV(\phi) + \frac{W_{\theta}^2}{2} g(\phi) |\nabla\theta|^2 \right] dV, \quad (2)$$

where W_{ϕ} and W_{θ} are gradient energy coefficients, H scales the single-well potential $V(\phi)$,
45 and $g(\phi)$ is a coupling function that diverges at $\phi = 1$. This divergence plays two roles: firstly localizing the gradient in orientation to a finite width GB, and secondly, preventing changes to the orientation field outside of the GB region. The latter amounts to removing grain rotations from the model, by creating an infinite driving force against rotation in the bulk crystal where $\phi = 1$. This model was adopted to simulate grain growth using a single-
50 well potential $V(\phi)$, and properties such as triple junction angles and steady-state velocities were verified using simulations [7].

Both the KWC and HMP models contain an explicit dependence of the GB energy on the

¹. Generally speaking, the model predicts the grain boundary *free* energy, but we will refer to it as grain boundary energy for brevity.

gradient in orientation, preventing fully arbitrary misorientation dependence of the boundary energy without further modification. Previous work has demonstrated methods for introducing dependence of the GB energy on inclination and misorientation axis [6]; however, the GB energy still increases with misorientation angle for a given inclination and misorientation axis. In Section 2, we show analytically that the GB energy must increase monotonically with misorientation in both model formulations. This is a fundamental limitation, and it prevents the modeling of both isotropic GB energies (the so-called soap froth problem) and, more importantly, realistic polycrystalline materials, where there are often multiple minima in the boundary energy.

In this work, we propose an alternative formulation for the KWC model, motivated by the preceding analysis, which introduces a dependence of the model coefficients on a nonlocal measure of GB misorientation. This choice is inspired by the work of Han and van de Walle [8], who formulate a new orientation-field model and an iterative algorithm for computing misorientation non-locally. In Section 3, we provide the modified KWC model equations and an algorithm to rapidly compute nonlocal misorientation. We discuss the introduction of misorientation dependence of the GB energy, as well as adjustment of the orientation-field mobility to prevent grain rotation (“plateau motion”). In Section 4, we examine the energy and mobility of GBs in the model and demonstrate the ability of the model to capture sharp cusps in GB energy. Finally, we describe a 3D extension to the model in Section 5, and present our conclusions in Section 6.

2 Theory

2.1 Equilibrium Bicrystal Solutions

75 The goal of this section is to provide an analytical result for the GB energy as a function of misorientation for the case of a single planar GB located at the center of an infinite one-dimensional domain. The bulk crystal orientations are θ_1 and θ_2 in the left and right halves of the domain, respectively. The order parameter ϕ is $\phi = 1$ in the bulk crystal and decreases near the boundary. We assume that the order parameter profile $\phi(x)$ has a single
80 minimum in the GB region, while the misorientation profile $\theta(x)$ is a monotonic function of the coordinate x . The boundary conditions are summarized as follows, where the subscript x indicates the derivative with respect to position:

$$\lim_{x \rightarrow -\infty} \theta(x) = \theta_1, \quad (3)$$

$$\lim_{x \rightarrow +\infty} \theta(x) = \theta_2, \quad (4)$$

$$\lim_{x \rightarrow \pm\infty} \phi(x) = 1. \quad (5)$$

85 In addition to these boundary conditions, the potential is zero in the bulk crystal, $V(1) = 0$, so the only contribution to the free energy is due to the presence of the planar GB. The free energy contribution from the GB is positive, so $V(\phi) > 0$; these are the only constraints imposed on the potential. No assumptions are made about the form of $g(\phi)$ and $h(\phi)$.

To determine the change in GB energy with misorientation in the KWC model, we begin by
 90 finding the equilibrium profiles and corresponding free energy for an arbitrary misorientation
 that is set by the boundary conditions. Much of this derivation can be found in Appendix
 A of Warren et al. [3]. We adopt the convention of x -subscripts for the spatial derivatives of
 ϕ and θ , i.e. $\phi_x \equiv d\phi/dx$, $\phi_{xx} \equiv d^2\phi/dx^2$, and $\theta_x \equiv d\theta/dx$. We retain d/dx for more general
 differentiation with respect to x . The Euler-Lagrange equations for the KWC model in one
 95 dimension are:

$$0 = \frac{\delta F}{\delta \phi} = \frac{dV}{d\phi} + s \frac{dg}{d\phi} |\theta_x| + \frac{\epsilon^2}{2} \frac{dh}{d\phi} (\theta_x)^2 - \alpha^2 \phi_{xx} \quad (6)$$

and

$$0 = \frac{\delta F}{\delta \theta} = \frac{d}{dx} [sg(\phi)\theta_x |\theta_x|^{-1} + \epsilon^2 h(\phi)\theta_x]. \quad (7)$$

The first integral, a direct consequence of Noether's theorem [22], of the system is found to
 be

$$V(\phi) - \frac{\alpha^2}{2} (\phi_x)^2 - \frac{\epsilon^2}{2} h(\phi) (\theta_x)^2 = 0. \quad (8)$$

The θ equation, Eq. (7), can be trivially integrated once, introducing a constant of integra-
 100 tion C :

$$C = sg(\phi)\theta_x |\theta_x|^{-1} + \epsilon^2 h(\phi)\theta_x. \quad (9)$$

This equation can be written as

$$C = \pm sg(\phi) + \epsilon^2 h(\phi)\theta_x, \quad (10)$$

where we use the positive sign if $\Delta\theta \equiv \theta_2 - \theta_1 > 0$ and the negative if $\Delta\theta < 0$. Solving for θ_x , we find

$$\theta_x = \frac{C \mp sg(\phi)}{\epsilon^2 h(\phi)}. \quad (11)$$

Equations (8) and (11) show that the profiles must possess the following symmetries: $\phi(x) =$
 105 $\phi(2\zeta_0 - x)$ and $\theta_x(x) = \theta_x(2\zeta_0 - x)$, where ζ_0 is the coordinate of the minimum of $\phi(x)$. Indeed, Eq.(11) shows that at points with the same ϕ on either side of the minimum, θ_x must be the same, while according to Eq.(8), at such points the derivatives ϕ_x have the same magnitude with opposite signs.

It has been shown [3] that the misorientation profile $\theta(x)$ is localized in a finite interval
 110 $\zeta_1 \leq x \leq \zeta_2$ that covers the GB core with $\theta_x \equiv 0$ outside this interval. In contrast, the order-parameter profile $\phi(x)$ has diffuse tails that extend outside the interval of nonzero $|\theta_x|$ values. Consequently, solutions are sought in three regions: the inner region $[\zeta_1, \zeta_2]$ and two outer regions $[-\infty, \zeta_1]$ and $[\zeta_2, \infty]$. By the symmetry of the profiles,

$$\phi(\zeta_1) = \phi(\zeta_2) \equiv \phi_{max} \quad (12)$$

Since at the end points of the inner region $\theta_x = 0$ and $\phi = \phi_{max}$, we have from Eq.(11):

$$C = \pm sg(\phi_{max}). \quad (13)$$

115 This allows us to rewrite Eq.(10) as

$$\theta_x = \pm \frac{sg(\phi_{max}) - sg(\phi)}{\epsilon^2 h(\phi)}. \quad (14)$$

In the outer region, because $\theta_x = 0$,

$$\frac{\alpha^2}{2} (\phi_x)^2 = V(\phi). \quad (15)$$

giving a direct relationship between the spatial variation in ϕ and the potential. However, to obtain ϕ_x in the inner region, we substitute Eq. (14) into Eq. (8) and find

$$\frac{\alpha^2}{2} (\phi_x)^2 = V(\phi) - \frac{s^2}{2\epsilon^2} \frac{(g(\phi_{max}) - g(\phi))^2}{h(\phi)}. \quad (16)$$

Applying this equation to the minimum of the order parameter, we have

$$V(\phi_0) = \frac{s^2}{2\epsilon^2} \frac{(g(\phi_{max}) - g(\phi_0))^2}{h(\phi_0)}. \quad (17)$$

120 On the other hand, we integrate Eq.(14) through the inner region:

$$\int_{\zeta_1}^{\zeta_2} \theta_x dx = \Delta\theta = \pm \int_{\zeta_1}^{\zeta_2} \left[\frac{sg(\phi_{max}) - sg(\phi)}{\epsilon^2 h(\phi)} \right] dx = \pm \int_{\zeta_1}^{\zeta_2} \left[\frac{sg(\phi_{max}) - sg(\phi)}{\epsilon^2 h(\phi)} \right] \frac{dx}{d\phi} d\phi. \quad (18)$$

Inserting ϕ_x from Eq.(15), we have

$$\Delta\theta = \pm \frac{\sqrt{2}\alpha s}{\epsilon^2} \int_{\phi_0}^{\phi_{max}} \frac{g(\phi_{max}) - g(\phi)}{\epsilon^2 h(\phi) \sqrt{V(\phi) - \frac{s^2 [g(\phi_{max}) - sg(\phi)]^2}{2\epsilon^2 h(\phi)}}} d\phi \quad (19)$$

Equations (17) and (19) establish a relationship between the minimum/maximum order parameters ϕ_0 and ϕ_{max} and $\Delta\theta$ [3]. Knowing ϕ_0 and ϕ_{max} , the boundaries of the inner region can be found from [3]

$$\zeta_2 = \zeta_0 + \frac{\alpha}{\sqrt{2}} \int_{\phi_0}^{\phi_{max}} \frac{d\phi}{\sqrt{V(\phi) - \frac{s^2 [g(\phi_{max}) - sg(\phi)]^2}{2\epsilon^2 h(\phi)}}} \quad (20)$$

125 and $\zeta_1 = 2\zeta_0 - \zeta_2$.

2.2 Dependence of grain boundary energy on $\Delta\theta$

Of particular interest is the change of γ_{GB} with respect to the misorientation, $\Delta\theta$. We assume that the system is configured as detailed above, with the GB centered at $x = \zeta_0$.

The analysis holds for the KWC and HMP models. We define a function w to represent the

130 argument of Eq. (1), writing

$$\gamma_{GB} = \int_{\zeta_1}^{\zeta_2} w(\theta_x(x), \phi(x), \phi_x(x)) dx + \int_{-\infty}^{\zeta_1} w(\phi(x), \phi_x(x)) dx + \int_{\zeta_2}^{\infty} w(\phi(x), \phi_x(x)) dx \quad (21)$$

with the following boundary conditions: $\theta_x = 0$ at $x \leq \zeta_1$ and $x \geq \zeta_2$, and $\theta(\zeta_2) - \theta(\zeta_1) = \Delta\theta$. Note that we have omitted θ_x from the arguments of w outside the range $\zeta_1 \leq x \leq \zeta_2$ where θ_x is 0.

We revisit the variational derivative formally, now retaining the boundary terms, as this is precisely what we are interested in varying (specifically $\Delta\theta$). These give natural boundary conditions for the first variation in the GB free energy that specify the values of θ at each end of the domain. This is critical in setting the dependence of the GB energy on misorientation.

The first variation of the GB energy is

$$\begin{aligned}
\delta\gamma_{GB} &= \int_{\zeta_1}^{\zeta_2} \left[\left(-\frac{d}{dx} \frac{\partial w}{\partial \theta_x} \right) \delta\theta + \left(\frac{\partial w}{\partial \phi} - \frac{d}{dx} \frac{\partial w}{\partial \phi_x} \right) \delta\phi \right] dx \\
&+ \int_{-\infty}^{\zeta_1} \left[\left(\frac{\partial w}{\partial \phi} - \frac{d}{dx} \frac{\partial w}{\partial \phi_x} \right) \delta\phi \right] dx + \int_{\zeta_2}^{\infty} \left[\left(\frac{\partial w}{\partial \phi} - \frac{d}{dx} \frac{\partial w}{\partial \phi_x} \right) \delta\phi \right] dx \\
&+ \frac{dw}{d\theta_x} \delta\theta \Big|_{\zeta_1}^{\zeta_2} + \frac{dw}{d\phi_x} \delta\phi \Big|_{\zeta_1}^{\zeta_2} + \frac{dw}{d\phi_x} \delta\phi \Big|_{-\infty}^{\zeta_1} + \frac{dw}{d\phi_x} \delta\phi \Big|_{\zeta_2}^{\infty} \\
&+ w(\theta_x(\zeta_2), \phi(\zeta_2), \phi_x(\zeta_2))\delta\zeta_2 - w(\theta_x(\zeta_1), \phi(\zeta_1), \phi_x(\zeta_1))\delta\zeta_1 \\
&+ w(\phi(\zeta_1), \phi_x(\zeta_1))\delta\zeta_1 - w(\phi(\zeta_2), \phi_x(\zeta_2))\delta\zeta_2.
\end{aligned} \tag{22}$$

Note that we included variations of the boundaries ζ_1 and ζ_2 of the three regions discussed in the previous section. This was necessary because these boundaries are related to the angles of misorientation through equations (17) and (19)-(20). The integrals in Eq. (22) are, of course, zero. Also, $dw/d\phi_x = \alpha^2\phi_x \rightarrow 0$ at $x \rightarrow \pm\infty$. To preserve the symmetry of the order parameter profile, the variations $\delta\phi$ at ζ_1 and ζ_2 must be equal. As a result, the terms with $\delta\phi$ cancel mutually.

145 In the last two lines of Eq.(22), the pairs of terms with $\delta\zeta_1$ and $\delta\zeta_2$ mutually cancel because $\theta_x = 0$ at ζ_1 and ζ_2 , and therefore

$$w(\theta_x(\zeta_1), \phi(\zeta_1), \phi_x(\zeta_1)) = w(\phi(\zeta_1), \phi_x(\zeta_1)), \quad (23)$$

$$w(\theta_x(\zeta_2), \phi(\zeta_2), \phi_x(\zeta_2)) = w(\phi(\zeta_2), \phi_x(\zeta_2)). \quad (24)$$

We are left with the following equation:

$$\delta\gamma_{GB} = \left. \frac{dw}{d\theta_x} \delta\theta \right|_{\zeta_1}^{\zeta_2}. \quad (25)$$

We are reminded from Eq. (7) that $\partial w/\partial\theta_x = C$, and therefore

$$\delta\gamma_{GB} = C \delta\theta \left|_{\zeta_1}^{\zeta_2} = C[\delta\theta_{x=\zeta_2} - \delta\theta_{x=\zeta_1}]. \quad (26)$$

150 Importantly for this analysis, $\delta\theta_{x=\zeta_2} - \delta\theta_{x=\zeta_1} = \delta(\Delta\theta)$, from which

$$\delta\gamma_{GB} = C\delta(\Delta\theta). \quad (27)$$

In the KWC model, $C = \pm sg(\phi_{max})$. It would be a different constant for the HMP model, but the variation of the energy with respect to θ must be constant because it lacks a dependence on θ , only θ_x . Thus, for the KWC model we have

$$\delta\gamma_{GB} = \pm sg(\phi_{max})\delta(\Delta\theta). \quad (28)$$

In other words,

$$\frac{d\gamma_{GB}}{d|\Delta\theta|} = sg(\phi_{max}). \quad (29)$$

155 Equation (29) shows that the GB energy must remain constant or increase with misorientation in the KWC model. In fact, as the above approach is quite general, particularly from Eq. (22), it can be generalized to other orientation-field models. This result precludes the application of orientation-field models to isotropic systems (i.e., one cannot generally simulate the “soap-froth” problem with an orientation-field model). In addition, cusps in the GB energy
160 at special misorientations cannot be reproduced without further modification of the model’s free energy functional. On the basis of these conclusions, polycrystalline systems with an arbitrary five-dimensional dependence of the GB energy on GB crystallography cannot be modeled using such, as formulated, orientation-field models.

In order to remedy this situation, we considered a number of methods by which the limitation
165 imposed by Eq. (29) could be circumvented or eliminated, including introducing additional order parameters, allowing $V(\phi)$, $g(\phi)$, and/or $h(\phi)$ to take negative values, and introducing higher-order terms in $\nabla\theta$. However, each of these methods introduces new problems, such as limiting the range of $\Delta\theta$ for which equilibrium solutions exist or dramatically increasing the mathematical and computational complexity. Instead, we argue that the root of the problem
170 is the non-locality of information required to determine GB misorientation.

If a GB is defined as a diffuse region over which θ changes from one constant value to another, the misorientation can be computed by integrating $\nabla\theta$ along the GB normal direction, \vec{n} ,

through the entire diffuse boundary region, $-d < l < +d$, $\nabla\theta(\pm d) = 0$:

$$\Delta\theta = \int_{-d}^{+d} \nabla\theta \cdot \vec{n} dl = \theta(\vec{x} + d\vec{n}) - \theta(\vec{x} - d\vec{n}). \quad (30)$$

If, as is often assumed in phase-field models, the diffuse interface width is greater than the
175 discrete elements on which the solution is represented ($d \gg \Delta x$), then the misorientation is
a nonlocal quantity compared to the local energy density typically considered in phase-field
models. Although there is a relationship between $\nabla\theta$ and $\Delta\theta$, $\Delta\theta$ cannot be calculated from
 $\nabla\theta$ at only a single point where the equations are numerically integrated. However, based
on the (potentially incomplete) prevailing theory of grain growth, $\Delta\theta$ should determine the
180 GB energy rather than $\nabla\theta$.

To reconcile this, we propose introducing a dependence on the nonlocal misorientation to the
KWC model's coupling coefficients, s and ϵ . This idea is inspired by the recent model of Han
and van de Walle [8], in which the nonlocal misorientation was introduced and an iterative
search algorithm was proposed to calculate it. In the following section, we introduce the
185 nonlocal misorientation to the KWC model and describe an algorithm to calculate $\Delta\theta$.

3 Methods

3.1 Model

The free energy functional of the KWC model (Eq. (1)) is modified by introducing a dependence on the nonlocal misorientation, $\Delta\theta$, as follows:

$$F[\phi, \theta] = \int_{\Omega} \left[V(\phi) + \frac{\alpha^2}{2} |\nabla\phi|^2 + s(\Delta\theta)g(\phi)|\nabla\theta| + \frac{s(\Delta\theta)^2\epsilon^2}{2} h(\phi)|\nabla\theta|^2 \right] dV. \quad (31)$$

190 Note that $\Delta\theta$ represents the nonlocal misorientation, not the Laplacian operating on θ . The choice to introduce a dependence of s on $\Delta\theta$ is motivated by Eq. (29): if $g(\phi)$ must increase monotonically, then s must be allowed to vary so that γ_{GB} can decrease or increase with misorientation.

The Euler-Lagrange equation for θ now involves variations in $\Delta\theta$; however, assuming that d is
 195 large enough to satisfy the condition $\nabla\theta(\vec{x} \pm d\vec{n}) = 0$, the variation in nonlocal misorientation is zero to first order [8]. Then, the evolution equations closely resemble those of the KWC model:

$$\frac{\partial\phi}{\partial t} = M_{\phi} \frac{\delta F}{\delta\phi} = M_{\phi} \left[V'(\phi) + s(\Delta\theta)g'(\phi)|\nabla\theta| + \frac{s(\Delta\theta)^2\epsilon^2}{2} h'(\phi)|\nabla\theta|^2 - \alpha^2 \nabla^2\phi \right] \quad (32)$$

and

$$\frac{\partial\theta}{\partial t} = M_{\theta} \frac{\delta F}{\delta\theta} = M_{\theta} \left[-\nabla \cdot \left(s(\Delta\theta)^2\epsilon^2 h(\phi)\nabla\theta + s(\Delta\theta)g(\phi) \frac{\nabla\theta}{|\nabla\theta|} \right) \right]. \quad (33)$$

3.2 Numerical treatment

200 To compute the nonlocal misorientation at a given point, two quantities must be determined:
the GB normal vector, \vec{n} , and “search distance”, d , which enters the bounds of the integral
in Eq. (30). The former can be determined based on $\nabla\theta$. The latter is more complex, as the
search distance should result in $\nabla\theta(\vec{x}\pm d\vec{n}) = 0$ for the point \vec{x} at which we are evaluating $\Delta\theta$.
Han and van de Walle [8] use an iterative search algorithm, wherein d depends on the θ field
205 and is chosen by incrementally advancing along \vec{n} until $\nabla\theta$ is less than a set “cutoff” value.
For bicrystals, this approach ensures that $\nabla\theta(\vec{x}\pm d\vec{n}) = 0$ is always satisfied. Within a triple
junction, if \vec{n} points along a planar GB, the iterative search algorithm will not terminate as
a region where $\nabla\theta(\vec{x} + d\vec{n}) = 0$ will never be reached. To avoid this problem, Han and van
de Walle set a maximum search distance for their algorithm.

210 The computational cost to compute $\Delta\theta$ can be significantly reduced by introducing a constant
search distance d . Treating d as a constant eliminates the iterative process and reduces the
number of 2D interpolations to the minimum number of 2 per evaluation of $\Delta\theta$. However, d
must be chosen to be large enough to cover the entire GB width while small enough to avoid
intersecting additional grain boundaries. For example, with d much larger than the GB width
215 and considering a circular grain embedded within a matrix, the nonlocal misorientation could
be incorrectly evaluated as zero if d is larger than the radius of the embedded grain.

We use the finite volume method to discretize Eqs. (32) and (33) in space, and perform
integration with respect to time by the method of lines using an explicit low-storage fourth-

order Runge-Kutta scheme with an embedded fifth-order scheme for adaptive time stepping
 220 [23, 24]. The model is implemented in a serial C++ code, which is sufficient to produce the
 results presented here. Parallelization of the nonlocal misorientation algorithm is challenging,
 as each processor requires long-range information about the θ field. The usual cartesian
 topology for an MPI implementation would require a layer of ghost points covering a region
 of at least d in size; alternatively, the entire θ field would need to be shared or broadcast
 225 among every processor. Parallel implementation of the model code is left for future work.

3.3 Parameterization

We adopt the following forms for $V(\phi)$, $g(\phi)$, and $h(\phi)$ from previous work [3]:

$$V(\phi) = \frac{a^2}{2}(1 - \phi)^2 \quad (34)$$

and

$$g(\phi) = h(\phi) = \phi^2. \quad (35)$$

Importantly, the functional form of $s(\Delta\theta)$ can be determined from the expression of the GB
 230 energy as a function of misorientation. In the limit where $\epsilon = 0$, Eq. (21) gives the GB
 energy as a function of ϕ_0 and $\Delta\theta$:

$$\gamma_{GB} = sg(\phi_0)\Delta\theta + 2\alpha \int_{\phi_0}^1 \sqrt{2V(\phi)}d\phi = s\phi_0^2\Delta\theta - 2a\alpha(1 - \phi_0). \quad (36)$$

When $\epsilon = 0$, Eq. (6) can be integrated to obtain ϕ_0 [2]:

$$\phi_0 = \frac{1}{1 + s\Delta\theta/a\alpha}. \quad (37)$$

Substituting Eq. (37) into Eq. (36) gives:

$$\gamma_{GB} = \frac{s\Delta\theta}{1 + s\Delta\theta/a\alpha}. \quad (38)$$

With some algebra, we obtain:

$$s(\Delta\theta) = \frac{\gamma_{GB}}{(1 - \gamma_{GB}/a\alpha)\Delta\theta}. \quad (39)$$

235 Using Eq. (39), we can embed arbitrary relationships between GB energy and misorientation, allowing the model to naturally capture features such as cusps and symmetry.

To demonstrate the capability of the model, we use the following expression for γ_{GB} in Eq. (39):

$$\gamma_{GB}(\Delta\theta) = \begin{cases} 0.1\Delta\theta + RS(\Delta\theta) \cdot RS(\frac{\pi}{2} - \Delta\theta) & 0 \leq \Delta\theta < \frac{\pi}{2} \\ 0.1\Delta\theta + RS(\pi - \Delta\theta) \cdot RS(\Delta\theta - \frac{\pi}{2}) & \frac{\pi}{2} < \Delta\theta < \pi \\ 0.1\Delta\theta & \Delta\theta = \frac{\pi}{2} \end{cases} \quad (40)$$

where $RS(x)$ is the following function that resembles the Read-Shockley dependence of GB
240 energy on misorientation for low angle GBs:

$$RS(x) = x(1 - \ln(x)). \quad (41)$$

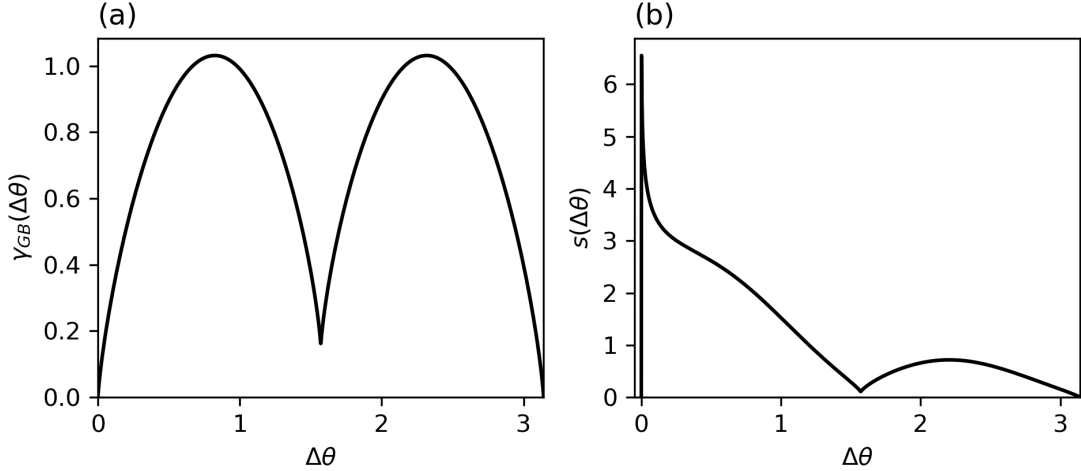


Figure 1: (a) Grain boundary energy function including a cusp at $\Delta\theta = \pi/2$ used in the present results. (b) Coefficient of the linear $\nabla\theta$ term as a function of nonlocal misorientation, $s(\Delta\theta)$, which results from Eq. 39 given the grain boundary energy function shown in (a).

Eq. 40 has a cusp at $\Delta\theta = \pi/2$ and is symmetric on $[0, \pi)$. When $\Delta\theta < 0$ or $\Delta\theta \geq \pi$, π is added to or subtracted from $\Delta\theta$ until $\Delta\theta \in [0, \pi)$. For the coefficient of the potential, we choose $a = \sqrt{2}$, and for the gradient energy coefficient in ϕ , we choose $\alpha = 2$. Figure 1 shows the value of $\gamma(\Delta\theta)$ and $s(\Delta\theta)$ using these parameters. Note that $s(\Delta\theta)$ is singular at $\Delta\theta = 0$; to avoid numerical problems, we add a small value (10^{-12}) to the denominator in Eq. (39). The coefficient of the term $(\nabla\theta)^2$ is $\epsilon = 0.5$ except where otherwise noted.

As in previous iterations of the KWC model [3], the θ mobility is divided by a function that is 1 above a small finite $|\nabla\theta|$ but tends to infinity as $|\nabla\theta|$ approaches zero:

$$M_\theta^{-1} = P(\epsilon|\nabla\theta|) = 1 - \exp(-\beta\epsilon|\nabla\theta|) + \frac{\mu}{\epsilon} \exp(-\beta\epsilon|\nabla\theta|), \quad (42)$$

where β and μ are constants that determine the “cut-off” in $|\nabla\theta|$. Modifying the mobility in this manner mitigates the so-called “elevator motion” where the orientation of bulk grains

changes far from the interface. Such a bulk rotation could not be accommodated in a real crystalline material and is therefore unphysical. For the constants in Eq. (42) we choose $\beta = 2000$ and $\mu = 10^4$. The grid spacing is $\Delta x = 0.1$, and the search distance for the nonlocal misorientation is $d = 3$ (30 voxels). Zero-flux boundary conditions are used for both ϕ and θ , and if the nonlocal misorientation search would extend beyond the simulation domain, the search would end at the point on the domain boundary intersected by the GB normal vector.

4 Simulation Results

4.1 Properties of planar grain boundaries

Equilibrium 1D profiles as a function of misorientation are determined by starting from constant ϕ and an initially sharp θ with the jump centered in the computational domain. The equilibrium profiles in ϕ have a minimum centered at the boundary, with the minimum value, ϕ_0 , increasing with γ_{GB} rather than with misorientation (Figure 2a). The θ profiles adopt the expected hyperbolic-tangent-like shape; however, it is important to note that the GBs have a truly finite width, where $\nabla\theta$ completely vanishes outside the diffuse interface region, rather than approaching zero in the limit towards infinity. The finite GB width varies with GB energy, increasing slightly as γ_{GB} decreases (Figure 2b). Because the dependence on $\Delta\theta$ was introduced to both $\nabla\theta$ -dependent terms in the free energy functional, the variation in GB width with GB energy is small (see Eq. A.13 in [3]). This ensures that a single

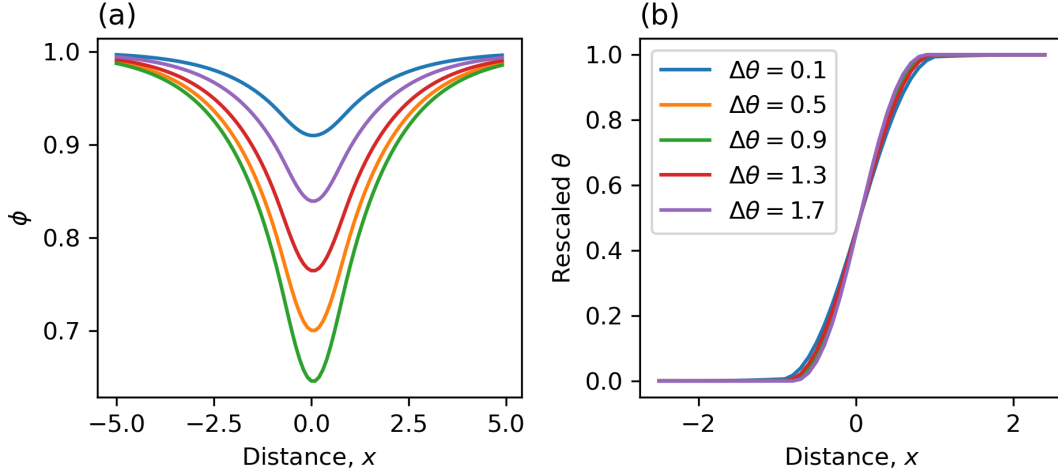


Figure 2: Equilibrium profiles for varying misorientation with $s(\Delta\theta)$ given by Eq. (39) with $\epsilon = 0.5$, for (a) ϕ and (b) θ . The colors described in the legend on (b) apply to both subfigures.

constant d can be chosen for the calculation of nonlocal misorientation. If the GB width
 were to vary more significantly, the nonlocal misorientation would need to be determined by
 an alternative algorithm, such as the iterative search of [8].

Given the equilibrium profiles, the GB energy can be numerically calculated and compared
 to the value expected based on Eq. (40). Figure 3 shows the comparison between the
 simulated GB energy and Eq. (40) for different values of ϵ . The derivation of Eq. 40
 involves inverting the relationship between γ_{GB} and $\Delta\theta$, which cannot be done analytically
 for $\epsilon \neq 0$. Therefore, the coefficient s based on Eq. 39 gives exactly the embedded γ_{GB}
 only for simulations with $\epsilon = 0$. As ϵ increases from zero, the GB energy in the simulations
 exceeds that specified by the input GB energy function. Because the KWC model requires
 nonzero ϵ for GBs to be mobile, the parameterization of GB energy in the present model
 still requires some calibration based on the selected ϵ to ensure that the desired $\gamma_{GB}(\Delta\theta)$ is
 accurately reproduced. Interestingly, $\gamma_{GB}(\Delta\theta)$ for $\epsilon > 0$ is well-approximated with a scalar

multiple of the $\epsilon = 0$ GB energy curve, which can be useful for accelerating the calibration process.

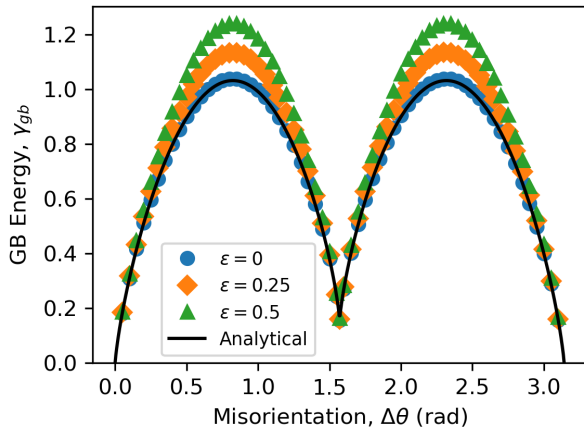


Figure 3: Grain boundary energy as a function of misorientation calculated from simulations of planar grain boundaries in 1D, compared to the input analytical function for $\gamma_{GB}(\Delta\theta)$ (Eq. (40)).

285 The chosen piecewise GB energy function, Eq. 40, has a cusp exactly at $\Delta\theta = \pi/2$, which is reproduced in the numeric computations of the 1D profiles without additional regularization or approximations. The presence of the cusp in the GB energy does not cause instability, since the cusp enters through the dependence on nonlocal misorientation, and the variation of θ with the nonlocal misorientation is zero. The ability to capture sharp cusps in GB

290 energy expands the applicability of the present KWC model to a wider variety of systems. In fact, as long as γ_{GB} goes to zero as $\Delta\theta = 0$, nearly-isotropic GB energy functions can be simulated; in theory, this allows the model to emulate the isotropic “soap-froth” problem for benchmarking comparisons with other phase-field approaches to simulating grain growth.

4.2 Circular grain boundaries

295 The GB mobility in the KWC model depends on both the misorientation and the model parameters and can be determined by asymptotic analysis in the limit $\epsilon \rightarrow 0$ [3]. We compute the GB mobility in our current model numerically by performing simulations of circular grains embedded in larger single crystal domains. The rate of change in the area A of the shrinking circular grain is related to the GB mobility by $dA/dt = -2\pi\gamma_{GB}\mathcal{M}$. The circular grain area is determined by normalizing θ by the misorientation, so that the inner grain elements are 1 and the matrix grain elements are 0; then, the sum of the normalized θ multiplied by Δx^2 gives the inner grain area. The GB mobility decreases with misorientation, diverging to infinity as $\Delta\theta \rightarrow 0$ (Figure 4).

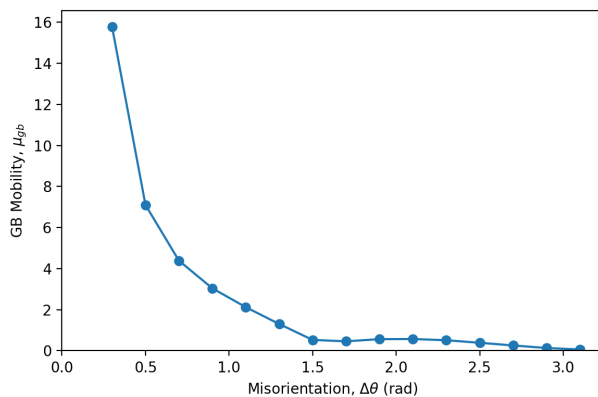


Figure 4: Grain boundary mobility as a function of misorientation, calculated from simulations of shrinking circular grains embedded in a matrix. Each point corresponds to a simulation; the line is to guide the eye.

The GB mobility decreases with misorientation, with a similar dependence on $\Delta\theta$ as $s(\Delta\theta)$ (compare Figure 4 to 1b). We make no claim on the physicality of this relationship, as GB mobility is a topic of current research; however, we posit that the dependence of GB mobility on misorientation in the model can be tuned by multiplicative composition of the θ mobility

coefficient, M_θ , with an appropriate function of $\nabla\theta$ and/or $\Delta\theta$. The details of adjusting the GB mobility are left for future work.

310 A more subtle feature of the KWC model is grain rotation, which can be reduced (but not completely eliminated) by adding the function $P(\epsilon|\nabla\theta|)$ to the θ mobility. What is important to emphasize, however, is that rotation can be controlled through this function, which can be used to dramatically slow evolution of the θ field in regions where $|\nabla\theta|$ is below a small value. With the present choice for μ and β , this value is approximately
315 $|\nabla\theta| \approx 0.01$. Because this value is not exactly zero, regions with small gradients in θ persist outside the diffuse GBs. These small regions can propagate from moving GBs, causing slow long-range grain rotations. The magnitude of the persistent small gradient does not depend on the macroscopic GB misorientation, so small-angle GBs are affected to a greater degree compared to high-angle GBs. With the parameters used in this work, migrating GBs with
320 misorientation below approximately 5° tend to adopt linear profiles with constant $|\nabla\theta| \approx 0.1$ spread over a wide region. Therefore, we do not calculate a mobility in Figure 4 for GBs with misorientation below 0.1 radian (5.7°).

5 3D Extension

Orientations in three dimensions have three degrees of freedom, necessitating the use of a
325 vector field to represent the orientation field. There are a number of possible representations for 3D rotations, including Euler angles, rotation matrices, axis-angle pairs, and Rodrigues

vectors [25, 26]. For computational efficiency, unit quaternions are ideal for extending the present model to 3D. A unit quaternion can be represented as a four-dimensional unit vector and describes a rotation of ψ degrees about an axis \hat{e} :

$$q_i = \begin{cases} \cos(\psi/2) & i = 0 \\ \hat{e}_i \sin(\psi/2) & i = 1, 2, 3 \end{cases} \quad (43)$$

330 A constraint must be introduced such that the norm of the quaternions remains unity.

The gradient in orientation can be replaced by the sum of squares of the quaternion components, which maintains rotational invariance. More complex forms for local misorientation can be derived that relate to the local misorientation axis and angle [6, 27]; however, these forms are not necessary when introducing nonlocal misorientation. The misorientation between two orientations represented by quaternions is simply $\mathbf{q}\mathbf{q}^{-1}$, where \mathbf{q}^{-1} is the inverse of \mathbf{q} , allowing straightforward insertion into the free energy functional:

$$F[\phi, \theta] = \int_{\Omega} \left[V(\phi) + \frac{\alpha^2}{2} |\nabla\phi|^2 + s(\mathbf{q}\mathbf{q}^{-1})g(\phi) \sum_{i=0}^3 |\nabla q_i| + \frac{\epsilon^2 s(\mathbf{q}\mathbf{q}^{-1})^2}{2} h(\phi) \sum_{i=0}^3 |\nabla q_i|^2 \right] dV. \quad (44)$$

The coefficient s becomes a function of 3D misorientation, with domain $SO(3)$. The symmetrized hyperspherical harmonics described by Mason and Schuh [28] can be employed to construct functions on $SO(3)$ with the appropriate symmetries.

340 Evaluation of the nonlocal misorientation requires the grain boundary normal vector, which was expressed as $\hat{n} = \nabla\theta/|\nabla\theta|$ in 2D. In the 3D model, the order parameter can be used to

compute the normal vector: $\hat{n} = \nabla\phi/|\nabla\phi|$. Alternatively, rotationally-invariant expressions involving the 3D orientation field can be derived for the local inclination vector [6]. The 2D bilinear interpolation of the orientation field must be replaced by a spherical interpolation
345 of quaternions.

6 Conclusions

We have presented a proof that orientation-field models for grain coarsening (including the Kobayashi-Warren-Carter and Henry-Mellenthin-Plapp models) cannot simulate the GB free energy decreasing with misorientation, limiting their applicability to simulating polycrys-
350 talline materials with energy cusps at special boundaries. We demonstrate a method to overcome this limitation by introducing a misorientation dependence of the orientation coupling coefficient, where the misorientation is determined by a line integral through the diffuse boundary width. This measure of misorientation requires evaluating the orientation on either side of the diffuse boundary, which we achieve (inspired by the work of Han and van
355 de Walle) by interpolating the orientation field at a constant distance along both directions of the GB normal vector. We apply this approach to the KWC model and demonstrate the capacity of the modified model to embed GB free energies as arbitrary functions of misorientation. The modified model allows for sharp cusps in the GB free energy as a function of misorientation, expanding the applicability of the KWC model to grain growth in polycrys-
360 talline materials with non-monotonic GB free energy. Because the form of the free energy function corresponds closely to the KWC model, many “tricks” for performing KWC simu-

lations are readily adapted to the present work, including the suppression of grain rotation and handling of topological defects. Finally, we propose a straightforward 3D extension of the model using quaternions to represent the orientation field and hyperspherical harmonic
365 functions to embed the misorientation-dependence of the GB free energy. Future model improvements could include alternate methods for calculating nonlocal misorientation (such as by image segmentation), incorporation of inclination dependence, and parallelization of the numerical method used to integrate the evolution equations.

Acknowledgments

370 This research was supported by the National Institute for Standards and Technology through the Center for Hierarchical Materials Design at Northwestern University contract [70NANB19H00]. This research was supported in part through the computational resources and staff contributions provided for the Quest high performance computing facility at Northwestern University which is jointly supported by the Office of the Provost, the Office for
375 Research, and Northwestern University Information Technology.

References

- [1] R. Kobayashi, J.A. Warren, and W.C. Carter. Vector-valued phase field model for crystallization and grain boundary formation. *Physica D: Nonlinear Phenomena*, 119(3-4):415–423, 1998.
- 380 [2] J.A. Warren, R. Kobayashi, and W.C. Carter. Modeling grain boundaries using a phase-field technique. *Journal of Crystal Growth*, page 3, 2000.
- [3] J.A. Warren, R. Kobayashi, A.E. Lobkovsky, and W.C. Carter. Extending phase field models of solidification to polycrystalline materials. *Acta Materialia*, 51:6035–6058, 2003.
- 385 [4] H. Henry, J. Mellenthin, and M. Plapp. Orientation-field model for polycrystalline solidification with a singular coupling between order and orientation. *Physical Review B*, 86:054117, 2012.
- [5] B. Korbuly, M. Plapp, H. Henry, J.A. Warren, L. Gránásy, and T. Pusztai. Topological defects in two-dimensional orientation-field models for grain growth. *Physical Review E*, 96:052802, 2017.
- 390 [6] N.C. Admal, J. Segurado, and J. Marian. A three-dimensional misorientation axis- and inclination-dependent Kobayashi–Warren–Carter grain boundary model. *Journal of the Mechanics and Physics of Solids*, 128:32–53, 2019.
- [7] P. Staublin, A. Mukherjee, J.A. Warren, and P.W. Voorhees. Phase-field model for anisotropic grain growth. *Acta Materialia*, 237, Sept 2022.
- 395

- [8] X. Han and A. van de Walle. A nonlocal orientation field phase-field model for misorientation- and inclination- dependent grain boundaries. *arXiv preprint*, 2025.
- [9] L.-Q. Chen and Y. Wang. The continuum field approach to modeling microstructural evolution. *JOM*, 48(12):13–18, 1996.
- 400 [10] D. Fan and L.-Q. Chen. Computer simulation of grain growth using a continuum field model. *Acta Materialia*, 45(2):611–622, 1997.
- [11] N. Moelans, B. Blanpain, and P. Wollants. Quantitative analysis of grain boundary properties in a generalized phase field model for grain growth in anisotropic systems. *Physical Review B*, 78(2):024113, 2008.
- 405 [12] I. Steinbach, F. Pezzolla, B. Nestler, M. Seeßelberg, R. Prieler, G.J. Schmitz, and J.L.L. Rezende. A phase field concept for multiphase systems. *Physica D: Nonlinear Phenomena*, 94(3):135–147, 1996.
- [13] I. Steinbach and F. Pezzolla. A generalized field method for multiphase transformations using interface fields. *Physica D: Nonlinear Phenomena*, 134(4):385–393, 1999.
- 410 [14] B. Nestler and A. Wheeler. Anisotropic multi-phase-field model: Interfaces and junctions. *Physical Review E*, 57(3):2602–2609, 1998.
- [15] H. Garcke, B. Nestler, and B. Stoth. A multiphase field concept: Numerical simulations of moving phase boundaries and multiple junctions. *SIAM Journal on Applied Mathematics*, 60(1):295–315, 1999.

- 415 [16] B. Nestler, H. Garcke, and B. Stinner. Multicomponent alloy solidification: Phase-field modeling and simulations. *Physical Review E*, 71(4):041609, 2005.
- [17] R. Folch and M. Plapp. Quantitative phase-field modeling of two-phase growth. *Physical Review E*, 72(1):011602, 2005.
- [18] S.G. Kim, D.I. Kim, W.T. Kim, and Y.B. Park. Computer simulations of two-
420 dimensional and three-dimensional ideal grain growth. *Physical Review E*, 74(6):061605, 2006.
- [19] I. Steinbach. Phase-field model for microstructure evolution at the mesoscopic scale. *Annual Review of Materials Research*, 43:89–107, 2013.
- [20] H. Kim, S.G. Kim, W. Dong, I. Steinbach, and B. Lee. Phase-field modeling for 3d
425 grain growth based on a grain boundary energy database. *Modelling and Simulation in Materials Science and Engineering*, 22(3):034004, 2014.
- [21] J. Zhang, W. Ludwig, Y. Zhang, H.H.B. Sørensen, D.J. Rowenhorst, A. Yamanaka, P.W. Voorhees, and H.F. Poulsen. Grain boundary mobilities in polycrystals. *Acta Materialia*, 191:211–220, 2020.
- 430 [22] I.M. Gelfand and S.V. Fomin. *Calculus of Variations*. Prentice-Hall, 1963.
- [23] J.H. Williamson. Low-storage runge-kutta schemes. *Journal of Computational Physics*, 35(1):48–56, 1980.

- [24] M.H. Carpenter and C.A. Kennedy. Fourth-order 2n-storage runge-kutta schemes. Technical Memorandum NASA/TM-109112, NASA, NASA Langley Research Center, Hampton VA 23681-0001, USA, June 1994.
- 435
- [25] A. Morawiec. *Orientations and Rotaitons: Computations in Crystallographic Textures*. Springer-Verlag Berlin Heidelberg, 2004.
- [26] D. Rowenhorst, A.D. Rollett, G.S. Rohrer, M. Groeber, M. Jackson, P.J. Konijnenberg, and M.D. Graef. Consistent representations of and conversions between 3d rotations. *Modelling and Simulation in Materials Science and Engineering*, 23(8):083501, 2015.
- 440 Publisher: IOP Publishing.
- [27] P. Staublin. *Orientation Field Model for Grain Growth Accounting for Five Crystallographic Degrees of Freedom*. PhD thesis, Northwestern University, 2024.
- [28] J.K. Mason and C.A. Schuh. Hyperspherical harmonics for the representation of crystallographic texture. *Acta Materialia*, 56(20):6141–6155, 2008.
- 445
- [29] N. Moelans, F. Wendler, and B. Nestler. Comparative study of two phase-field models for grain growth. *Computational Materials Science*, 46(2):479–490, 2009.